Synthesis, Modeling, and In Vitro Activity of (3′*S*)-*epi*-K-252a Analogues. Elucidating the Stereochemical Requirements of the 3′-Sugar Alcohol on trkA Tyrosine Kinase Activity

Diane E. Gingrich,[†] Shi X. Yang,[‡] George W. Gessner,[‡] Thelma S. Angeles,[‡] and Robert L. Hudkins*,[†]

Departments of Medicinal Chemistry and Biochemistry, Cephalon, Inc., 145 Brandywine Parkway, West Chester, Pennsylvania 19380

Received October 4, 2004

Utilizing our recently published semisynthetic approach to the (3′*S*)-K-252a diastereomer, we report the first synthesis of the (3′*R*)-**10** diastereomer and a set of related epimers, with the goal of defining the stereochemical role of the 3′-sugar hydroxyl group on trkA tyrosine kinase activity and selectivity. (3′*R*)-**10** displayed potent trkA inhibitory activity with an IC_{50} value of 4 nM. The corresponding deshydroxy epimer (3′*S*)-**14** was 7-fold more potent than its 3′*R* counterpart (natural stereochemistry) with a trkA IC_{50} value of 3 nM and demonstrated >280-fold selectivity over PKC (IC_{50} = 850 nM). In cells, (3′*S*)-**14** displayed potent inhibition of trkA autophosphorylation with an IC_{50} < 10 nM. Molecular modeling studies revealed that the 3′-OH, due to the inverted geometry, forms significant H-bonding interactions with Glu27 and Arg195, an interaction that is not attainable with the natural isomers.

Introduction

trkA is the high-affinity receptor-linked tyrosine kinase for the neurotrophin, nerve growth factor (NGF).[1] The receptor is composed of an extracellular NGF-binding domain, a single transmembrane sequence, and the cytoplasmic tyrosine kinase domain. NGF binding and receptor activation leads to receptor oligomerization and tyrosine phosphorylation of specific intracellular substrates such as PLCγ, PI3 kinase, ras, and raf/MEK/Erk1.[2] Tyrosine kinase activity is an absolute requirement for signal transduction through this class of receptor.

The role of the polypeptide growth factor NGF in the growth, differentiation, and survival of central and peripheral neurons is well established.[3] Whereas effective NGF/trkA signaling is important for neuronal systems, in the oncology field aberrant expression of NGF and trkA receptor kinase are implicated in the development and progression of human prostatic carcinoma and pancreatic ductal adrenocarcinoma.[4] NGF may also play a role in the development of breast cancer.[5] Accordingly, small molecule inhibitors of trkA tyrosine kinase have been proposed as a therapeutic approach for the treatment of prostate and pancreatic cancers, based on the premise that prostatic and pancreatic carcinoma cell growth utilize an NGF/trkA autocrine mechanism for continued proliferation.[4a,6] This hypothesis is currently being tested in the clinic with trkA inhibitors derived from the indolocarbazole (+)K-252a class.

The glycosylated indolocarbazole natural product (+)K-252a (**1**), isolated from *actinomadura*[7a] and *nocardiopsis* species K-252,[7b,c] is a potent ATP competitive inhibitor of trkA with an IC_{50} value of 13 nM.[8,9] Functionally, K-252a specifically inhibits NGF-induced autophosphorylation of trkA in cells without inhibiting βFGF, EGF, PDGF, or insulin-induced phosphorylation of their receptor kinases.[10] (+)K-252a also inhibits other NGF-induced events such as differentiation and survival of PC12 cells, neurite formation, and induction of c-fos.[11]

While (+)K-252a is a potent trkA inhibitor, its lack of selectivity and overt toxicity limit its usefulness as a drug. An ensuing medicinal chemistry program that was focused on optimizing the trkA activity on the (+)K-252a scaffold produced two compounds advancing into clinical evaluation: **2b** (CEP-2563), a water soluble Lys-βAla prodrug form for **2c** (CEP-751),[12] and **2a** (CEP-701)[6e,13] (Figure 1), a compound with improved oral bioavailability. **2a** and **2c** are potent trkA inhibitors with IC_{50} values of 4 nM and 3 nM, respectively. **2a** displays >100-fold selectivity against FGF-R1 and PDGF-Rβ, with modest selectivity against PKC (55-fold). In both rat and human prostate cancer models, **2a** significantly inhibited metastasis and growth of primary and metastatic tumors and showed significant induction of apoptotic death in tumor cells without toxicity to normal tissues. In 10 different prostate cancer animal models, **2a** significantly inhibited tumor growth independent of growth rate, hormone sensitivity, metastatic capability, or state of tumor differentiation.[4a,13] In the slow-growing androgen-sensitive Dunning H rat prostate tumor model, **2a** induced significant incidences of tumor regression independent of effects on cell cycle and in the absence of pronounced morbidity or toxicity following oral administration.[14] The aggressive behavior and poor prognosis of pancreatic ductal adrenocarcinoma contributes to the survival rate being one of the poorest for all cancers. The NGF-trk receptor axis has been implicated as the critical factor involved in the growth and progression of this disease.[4d] Preclinical studies with orally administered **2a** showed significant and selective inhi-

* To whom correspondence should be addressed. Phone 610-738-6283, e-mail rhudkins@cephalon.com.
[†] Department of Medicinal Chemistry.
[‡] Department of Biochemistry.

10.1021/jm040178m CCC: $30.25
Published on Web 05/03/2005

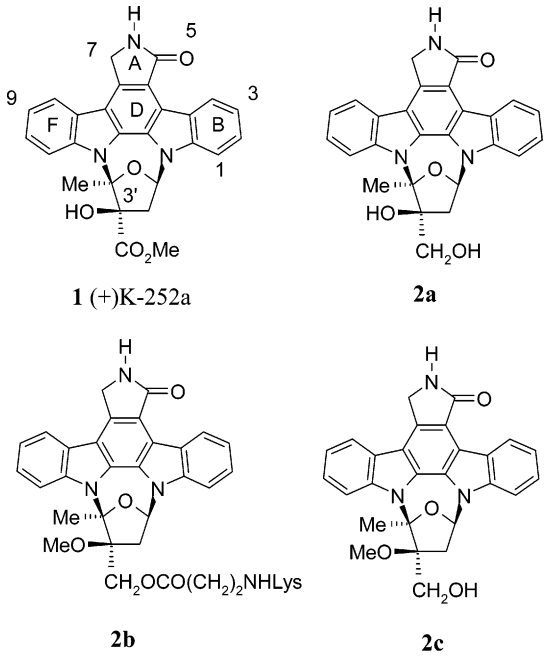

Figure 1. Structures of (+)-K-252a and advanced K-252a-derived analogues.

bition of tumor growth in six pancreatic xenograft models in the absence of toxicity.[4a,13]

Previous structure−activity relationship (SAR) studies from our labs involved elaborating the natural product (+)K-252a (2′*S*,3′*R*,5′*R* enantiomer).[15] The results from these studies revealed that substitution on positions 3 or 9 of aryl rings B and/or F typically reduced trkA activity, whereas the sugar 3′-position was important for modulating potency. In a preceding paper we reported an efficient semisynthetic approach to the (3′*S*)-K-252a diastereomer and its kinase profile.[16.] In this paper we describe SAR studies designed to further define the stereochemical role of the 3′-hydroxyl group on trkA activity and selectivity, including the first synthesis of the (3′*R*)-**10** diastereomer and a set of related 3′-epimers.

Synthetic Methods

Outlined in Schemes 1−3 are the routes to prepare the 3′-epimers. (3′*S*)-*epi*-K-252a was prepared as shown in Scheme 1.[16,17] Ketone **3** was prepared in 83% yield in two steps from (+)K-252a by lithium borohydride reduction to diol (3′*S*)-**2**, followed by periodic acid oxidative cleavage to **3**.[18] Inversion of the natural C-3 stereocenter was accomplished via cyanide attack to ketone **3** producing cyanohydrins (3′*S*)-**4a** and (3′*R*)-**4b**. Attempted isolation of **4a** and **4b** resulted in retrograde conversion back to the ketone. To circumvent this dilemma, the cyanohydrin intermediates were immediately subjected to a Pinner reaction, which produced (3′*S*)-**5** and a small amount of amide (3′*S*)-**6** isolated due to incomplete hydrolysis.

Shown in Scheme 2 are the synthetic routes to prepare (3′*R*)-**10** and its deshydroxy derivative (3′*S*)-**14**. Protection of (+)K-252a using TBSCl and DMAP in DMF produced the TBS-lactam. Lithium borohydride reduction to the protected diol was followed consecutively by thiocarbonate formation to intermediate **7** and Corey−Winter olefination using trimethyl phosphite to the exocyclic olefin intermediate **8**.[19] Osmylation of olefin **8** followed by deprotection of the TBS group using methanolic HCl produced (3′*R*)-**10**. The enantioselective approach to each methyl isomer (3′*S*)-**14** and (3′*R*)-**17** was through reductive ring opening of the pure chiral epoxides. Epoxide (3′*R*)-**12** was prepared from tosylate (3′*R*)-**11** using sodium hydride in THF. Treatment of (3′*R*)-**12** with lithium triethylborohydride followed by TBS deprotection generated (3′*S*)-**14**, the deshydroxyl methyl analogue of (3′*R*)-**10**. Scheme 3 outlines the synthetic route to the deshydroxyl methyl isomer (3′*R*)-**17** with the natural configuration. (3′*S*)-**2** was converted to the tosylate (3′*S*)-**15** (tosyl chloride, DMAP, CH_2Cl_2) then treated with sodium hydride to give the epoxide (3′*S*)-**16.** Lithium triethylborohydride reduction of epoxide **16** produced the chiral tertiary methyl alcohol (3′*R*)-**17**.

Results and Discussion

The kinase data for the K-252a analogues is shown in Table 1. The compounds were evaluated in a trkA enzyme-based assay utilizing an ELISA-based format[9] with time-resolved fluorescence readout and recombinant human phospholipase C-gamma/glutathione S-transferase fusion protein as a substrate. The primary objective was to establish the stereochemical preference of the 3′-OH on trkA activity and PKC selectivity by evaluating diastereomeric pairs of inhibitors. Since protein kinase C is involved in the transduction of a number of essential regulatory signals in the heart and has been linked to toxicity, the goal was to improve the PKC selectivity greater than 100-fold.[20] Compounds were also profiled against the angiogenesis target VEGF-R2, since **2a** displayed only about 16-fold separation and (+)K-252a is a potent inhibitor. As previously reported, the natural isomer (3′*R*)(+)K-252a **1** displays IC_{50} values of 13 nM for trkA, 250 nM for PKC, and 43 nM for VEGF-R2.[16] The K-252a 3′-epimer, (3′*S*)-**5**, was 11-fold more potent for trkA with an IC_{50} value of 1.2 nM and showed a 2- to 3-fold increase in potency for both PKC and VEGF-R2. The 3′-epi amide (3′*S*)-**6** was 24-fold weaker for trkA than the 3′-epi methyl ester **5** with an IC_{50} value of 29 nM. Compound **2a**, which contains the natural 3′*S* stereochemistry, is a 4 nM inhibitor of trkA with 55-fold selectivity over PKC. Inverting the 3′-chirality to (3′*R*)-**10** resulted in equivalent trkA activity. However, in a manner analogous to *epi*-**5**, inverting the 3′-OH increased the potency (decreased selectivity) for both PKC and VEGF-R2. (3′*R*)-**10** proved to be an exceptionally potent inhibitor of the angiogenesis target VEGF-R2 with an IC_{50} value of 4 nM.

While the K-252a epimers showed a clear preference for the 3′-OH stereochemistry for trkA, a similar comparison between diastereomers (3′*S*)-**2a** and (3′*R*)-**10** did not distinguish the isomers. The 3′-hydroxymethyl of **2a** may be more important and involved in a significant hydrogen bond analogous to the 3′-OH on (3′*R*)-**10**. The lactam N or O distance to the hydroxyl is < 0.5Å in both cases. **2c**, which differs from **2a** only by a 3′-methoxy vs 3′-OH group, displays equivalent trkA activity as **2a**, indicating the hydroxylmethyl may be the more critical functionality for trkA activity. To help clarify the contribution of the individual hydroxyl groups on diols

Scheme 1[a]

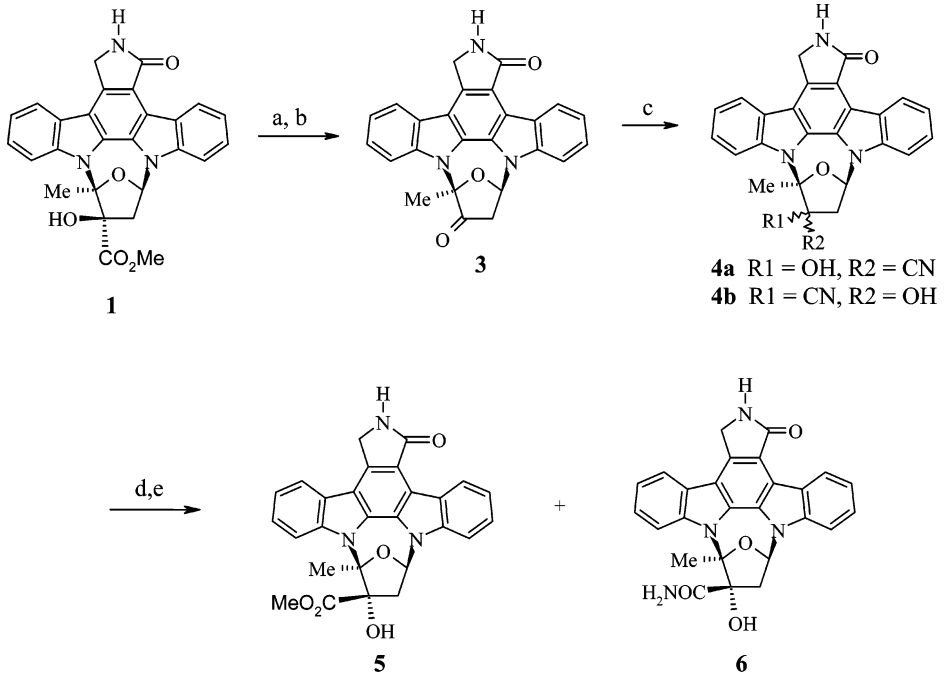

[a] Reagents and conditions: (a) $LiBH_4$, THF, rt, 81%; (b) H_5IO_6, THF, rt, 83%; (c) $^nBu_4NCN$, CH_2Cl_2, 0 °C−rt, 60%. (d) HCl_g, CH_3OH−dioxane; (e) 6 N HCl.

Scheme 2[a]

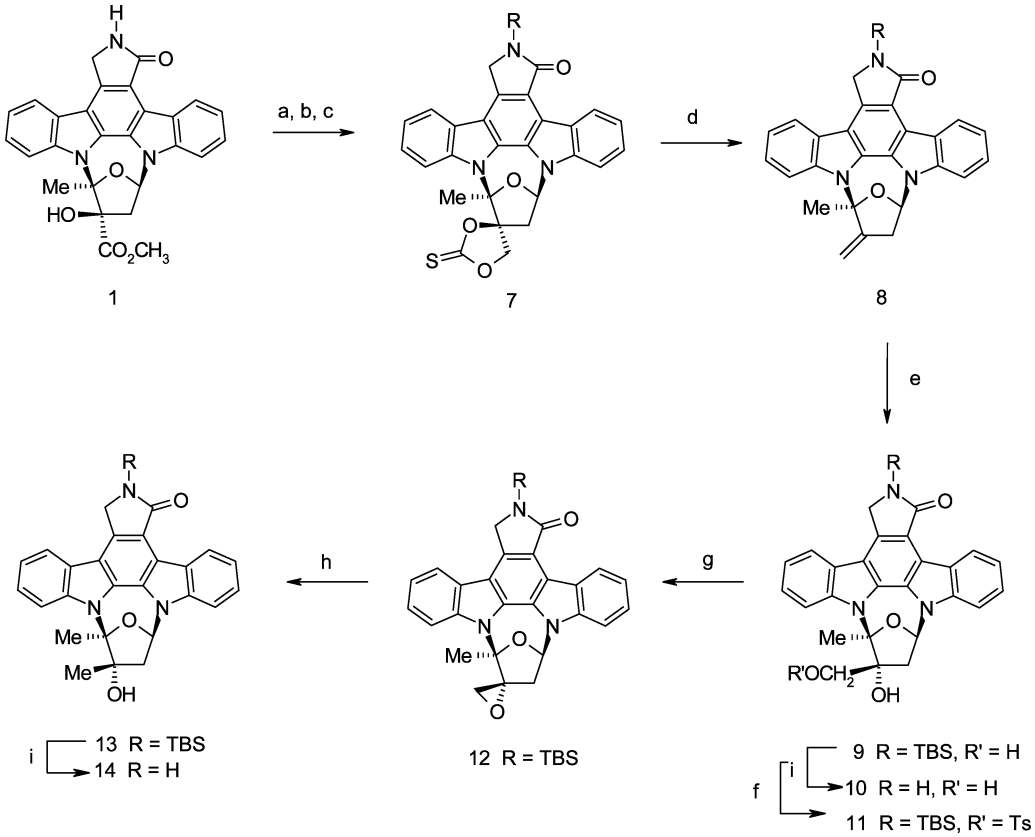

[a] Reagents and conditions: (a) TBSCl, DMAP, DMF (b) $LiBH_4$, THF, rt, 81% (c) NaH, CCl_2S, THF; (d) $P(EtO)_3$ (e) OsO_4 (f) Et_3N, pTsCl, (g) NaH, THF (h) lithium triethylborohydride (i) methanol, HCl.

(3′*S*)-**2** and (3′*R*)-**10** the deshydroxy isomers (3′*R*)-**17** and (3′*S*)-**14** were prepared. The (3′*R*)-**17** methyl compound with the natural 3′-configuration showed a 5-fold loss in trkA activity (IC_{50}= 20 nM) compared to diol (3′*S*)-**2a**. Conversely, methyl compound (3′*S*)-**14** with the unnatural configuration of the OH displayed equivalent activity compared to diol (3′*R*)-**10**, with a trkA IC_{50} of 3 nM. In addition, by removing the hydroxyl group (3′*S*)-**14** showed a 10-fold loss in PKC activity (IC_{50} = 850 nM), resulting in >280-fold selectivity against trkA.

Scheme 3[a]

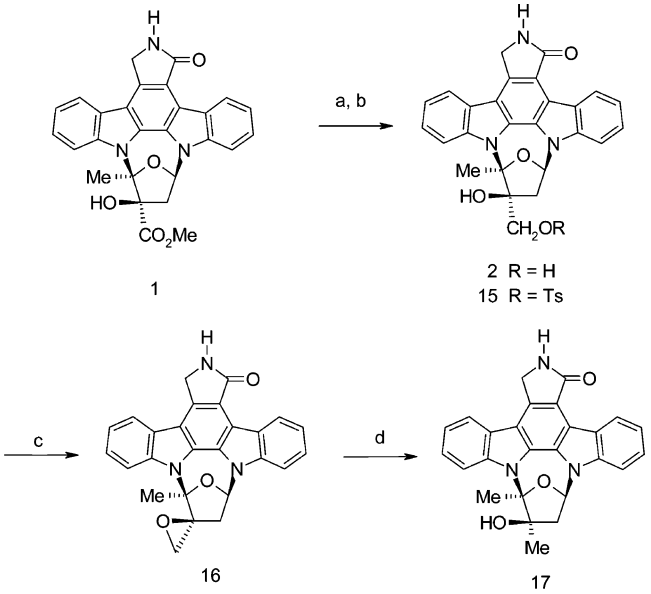

[a] Reagents and conditions: (a) lithium borohydride, THF; (b) *p*-toluenesulfonyl chloride, DMAP, CH_2Cl_2; (c) NaH, THF; (d) lithium triethylborohydride.

Table 1. Kinase Activity of (3′*R*)-**1** and (3′*S*)-**5** Analogues

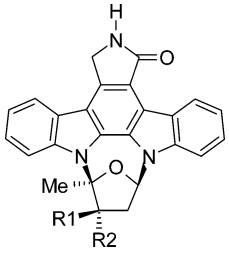

entry	R1	R2	trkA[a]	PKC[a]	VEGF-R2[a]	PKC/trkA
(3′-*R*)-**1**	OH	CO_2Me	13 ± 4	250	43 ± 16	19
(3′-*S*)-**5**	CO_2Me	OH	1.2 ± 0.2	114	19 ± 2	95
(3′-*S*)-**2a**	OH	CH_2OH	4 ± 1	218	65 ± 12	55
(3′-*R*)-**10**	CH_2OH	OH	4 ± 2	79	4 ± 1	20
(3′-*R*)-**17**	OH	Me	20 ± 2	310	76 ± 20	15
(3′-*S*)-**14**	Me	OH	3 ± 1	850	11 ± 3	283
(3′-*S*)-**6**	$CONH_2$	OH	29 ± 2	663	90 ± 24	23
(3′-*R*)-**2c**	OMe	CH_2OH	2.9 ± 0.3	114	–	39

[a] IC_{50} values are reported in nM. See Experimental Section for assay details. The trkA and VEGF-R2 assays were run in triplicate, the PKC value is the average of two determinations.

Analogous to isomers **5** and **10**, compound (3′*S*)-**14** showed a 7-fold increase in activity toward VEGF-R2. The key results generated from the methyl compounds support the conclusion that the geometry of the 3′-OH group is important for trkA activity and that the trans 3′-OH group below the sugar may possibly be involved in a significant H-bonding interaction.

Since trkA is an intracellular kinase it was important to establish the cell permeability of the epi-isomers. The compounds were evaluated in cells for dose-related inhibition of trkA autophosphorylation utilizing serum-starved NIH3T3 cells with varying concentrations of compound for 1 h at 37 °C.[21] The cells were stimulated with NGF followed by immunoprecipitation with an anti-trk antibody, probed with an antiphosphotyrosine antibody, and then detected by enhanced chemiluminescence. The results from the immunoblots are shown in Figure 2. The cellular IC_{50} for (3′*S*)-**5** was estimated

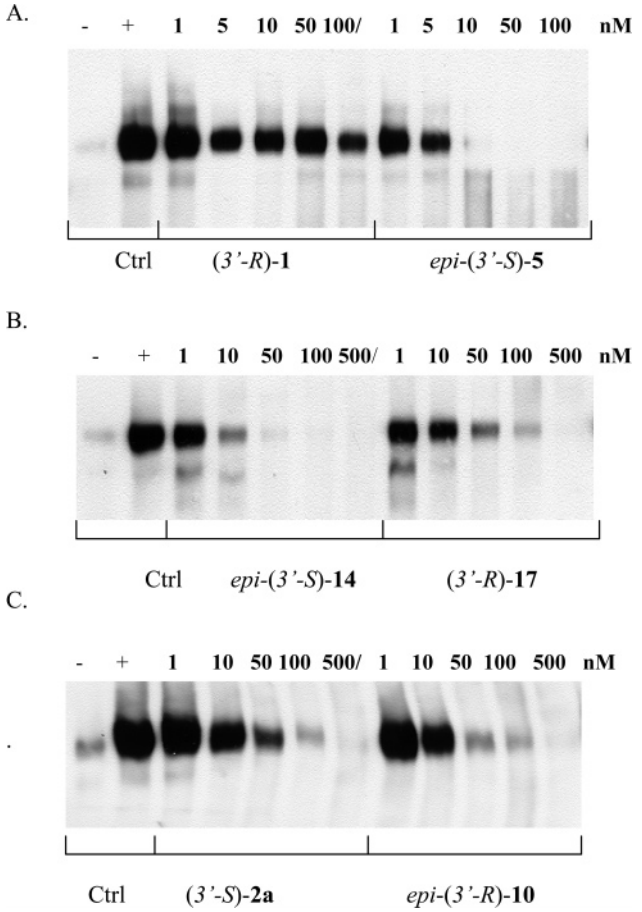

Figure 2. Inhibition of NGF-stimulated trkA phosphorylation in 3T3 cells.

to be ≅ 5 nM with complete inhibition at 10 nM, indicating that the compound is highly cell permeable and comparable to the IC_{50} of 1.2 nM in the isolated trkA kinase assay (Figure 2A). Alternatively, K-252a **1**, which displays an enzyme IC_{50} of 13 nM, does not show complete inhibition at 100 nM (Figure 2A). The methyl compound (3′*S*)-**14** demonstrated very high cell permeability with complete inhibition at 10 nM and <3-fold shift from the isolate enzyme IC_{50} (Figure 2B). The natural diol (3′*R*)-**2a** (IC_{50} = 4 nM) shows complete inhibition at 100 nM, while (3′*S*)-**10** (IC_{50} = 4 nM) shows complete inhibition at 50 nM (Figure 2B).

The significant conclusion from this study is the 3′-epi configuration of isomers (3′*S*)-**5** and (3′*S*)-**14** enhance potency at the trkA receptor, suggesting an additional receptor interaction due to the hydroxyl group geometry. Figure 3 depicts the geometry differences with energy minimized models of (+)K-252a **1** and *epi*-**5**. Structural insight into the trkA receptor binding interactions of the isomers is extremely valuable for the design of future potent and selective inhibitors. To gain some understanding of the binding differences between the natural and epi isomers, a homology model of trkA was constructed using its known sequence alignment with the average coordinates of three FGF-R1 inhibitor complexes (PDB codes 1FGI, 2FGI, 1AGW) as templates. FGF-R1 was identified from a BLAST search and displays 39% sequence identity to trkA. The model was built using the Composer module within Biopolymer in Sybyl 6.92 and renumbered from Thr1-Leu304. An initial 3D structure was obtained using the structurally

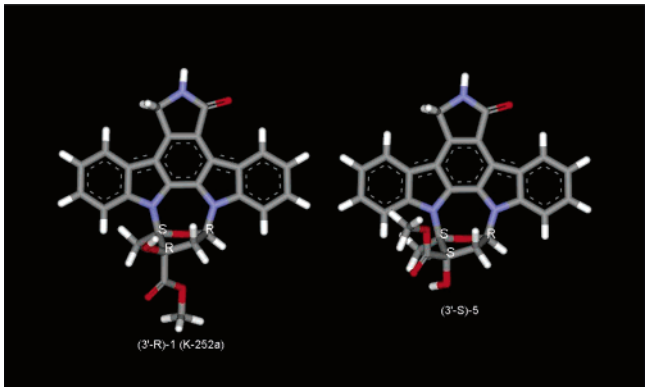

Figure 3. Energy-minimized models of (3′*S*)-**5** and (+)K-252a **1**.

conserved backbone regions. The structurally variable loop regions were then constructed from database searching of known kinase crystal structures. The refinement of the homology model was obtained through energy minimizations starting with a steepest descent (SD), then a conjugate gradient (CD) calculation using an MMFF94s force field to 0.05 kcal mol^{-1} $Å^{-1}$. The model was optimized further using a cycle of molecular dynamics calculations followed by an MMFF94s force field minimization. Within the trkA model, the coordinates of the ATP cavity were identified for docking studies by superimposing 1FGI and transferring the coordinates of the ATP-competitive oxindole inhibitor Su-5402. The cavity for docking studies was defined as 6.5 Å around SU-5402. The ATP-competitive docking mode of the indolocarbazole staurosporine natural product has been clearly established, with nine X-ray crystal structure complexes being solved. More recently, the crystal structure has been solved for (+)K-252a complexed with an unphosphorylated form of mutated c-Met kinase domain at 1.8 Å resolution (PDB code 1ROP).[22]

(3′*S*)-**5** was docked using the FlexX module within Sybyl 6.92 and minimized in the model. The docking mode including the significant H-bonding interactions with the trkA receptor is shown in Figure 4. This proposed model is consistent with the lactam moiety mimicking ATP with two key hydrogen bonds (donor and acceptor) anchoring the lactam to the hinge region as was reported with the K-252a/c-Met structure and with the staurosporine crystal structures. The lactam N−H shares a hydrogen with the Met101 backbone carbonyl (1.84 Å), while the lactam C=O hydrogen bonds with the backbone amide of Glu99 (1.65 Å). The sugar 3′-OH is involved in two hydrogen bonding interactions. An important feature of this trkA model, similar to that reported in FGF-R1 complexes,[23] is the glycine-rich nucleotide-binding loop adopts various conformations for ligand interactions. In this model the 3′-alcohol hydrogen shares a H-bond with the Glu27 carbonyl in the glycine rich loop (3.0 Å), while the alcohol oxygen forms a H-bond with Arg195 side chain from the C-terminal domain of the activation loop. Potential electrostatic contacts are feasible between the furan oxygen and Leu25 (3.22 Å), and the Arg163 backbone is in close proximity (3.24 Å) to the 3′-ester. Hydrogen bonding interactions are essential for ATP competitive kinase inhibitor binding, especially to the linker region, and contribute to additional potency as

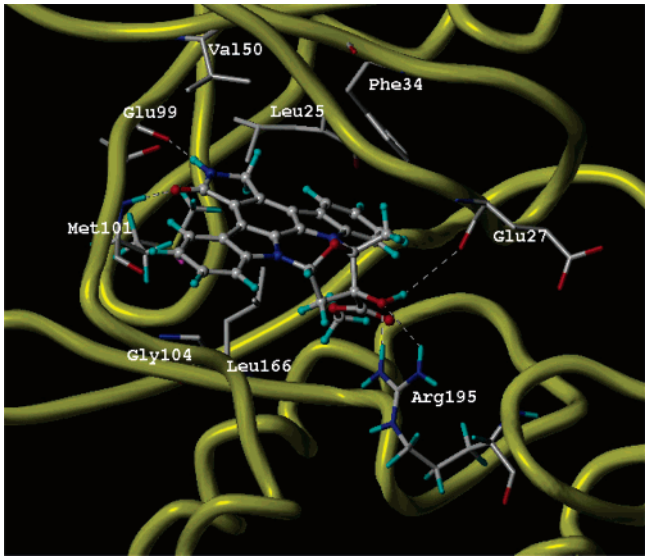

Figure 4. (3′*S*)-**5** docked in the trkA model showing important interactions.

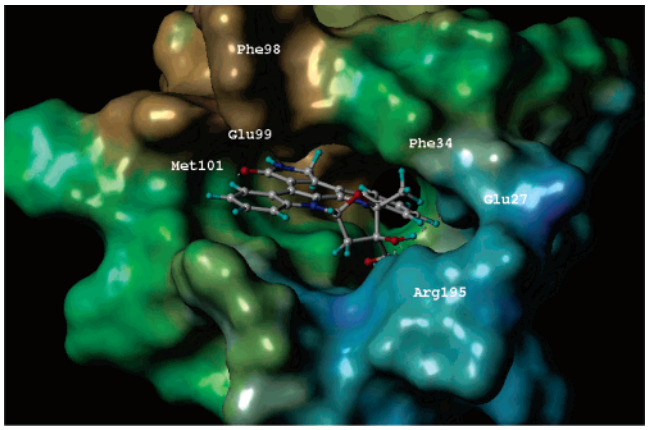

Figure 5. Hydrophobic surface map of the (3′*S*)-**5** trkA model.

shown with the *epi*-K-252a series. However, a significant amount of the binding energy in the indolocarbazole class is due to hydrophobic interactions. For example, the K-252a sugar moiety contributes significantly to the trkA activity through electrostatic interactions, but the aglycon K-252c retains good trkA potency with an IC_{50} value of 84 nM. In the trkA model the inhibitor is located in the hydrophobic ATP cavity with Phe98 and Tyr100 forming the base of the pocket. The F-ring phenyl group forms a favorable aromatic π-stacking interaction with the phenyl side chain of Phe34. The indolocarbazole makes significant van der Waals contacts with the surface of the pocket lined with residues Leu25, Ala29, Val50, Gly104, Cys165, Leu166, and Gly176. Figure 5 depicts a 6 Å hydrophobic surface map applied around (3′*S*)-**5**. An important feature is the binding of ring F of the indolocarbazole in a deep hydrophobic pocket formed by Phe34, with Asp177, Ile175, and Gly176 juxtaposed to the F-ring, while the B-ring is positioned on the border of the accessible solvent channel. Polar residues Arg102, Asp105, Asn107, and Arg108 line the solvent channel neighboring the 3-position.

In conclusion, we report the first synthesis of the (3′*R*)-**10**, and a set of related 3′-epimers, with the goal of defining the role of stereochemistry at the 3′-sugar

position on trkA tyrosine kinase activity and selectivity. The key results generated support the conclusion that the geometry of the 3′-OH group influences the trkA activity and selectivity. Whereas the diastereomer (3′*R*)-**10** showed potent trkA activity equivalent to the natural isomer with an IC_{50} of 4 nM, epi-isomers (3′*S*)-**5** and (3′*S*)-**14** were 7- and 13-fold more potent for trkA than the 3′*R* counterparts. In each case, the epimers were more potent for VEGF-R2. Methyl compound (3′*S*)-**14** was identified as a potent inhibitor of trkA with an IC_{50} of 3 nM and demonstrated >280-fold selectivity over PKC, a significant improvement over **2a**. In cells, (3′*S*)-**14** displayed potent inhibition of trkA autophosphorylation (IC_{50} < 10 nM), showing less than a 3-fold shift from the cell-free isolated enzyme assay. To aid in further understanding the molecular basis for the increased potency of the epimers, a homology model of trkA tyrosine kinase was constructed. Docking studies reveal that the 3′-OH, due to its geometry, is involved in significant H-bonding interactions with Glu27 and Arg195, not attainable with the 3′ natural stereochemistry enantiomers. Compound (3′*S*)-**14** showed good rat pharmacokinetic properties for further evaluation in trkA relevant models, which will be reported separately.

Experimental Section

Chemistry. All reagents and solvents were obtained from commercial sources and used as received. ^1H and ^{13}C NMR were obtained at 300 or 400 MHz in the solvent indicated with tetramethylsilane as an internal standard. Coupling constants (*J*) are in Hertz (Hz). Analytical HPLC was run using a Zorbax RX-C8, 5 × 150 mm column eluting with a mixture of acetonitrile and water containing 0.1% trifluoroacetic acid with a gradient of 10−100%. Column chromatography was performed on silica gel 60 (230−400 mesh). M-Scan Inc., West Chester, PA, performed high-resolution mass spectra (FAB).

Compound (3′*S*)-5. To a stirred solution of **3** (451 mg, 1.11 mmol) in CH_2Cl_2 (5 mL)-dioxane (1 mL) under nitrogen was added tetrabutylammonium cyanide (740 mg, 2.77 mmol) and acetic acid (95 μL, 1.66 mmol) at room temperature. The reaction mixture was stirred for 24 h, then concentrated in vacuo. The dark oil was dissolved in ethyl acetate (20 mL) and dioxane (2 mL) and washed with water (3 × 10 mL) and brine (1 × 10 mL). The organic phase was dried over magnesium sulfate, filtered, and concentrated in vacuo to a brown solid. This product was used immediately in the next step without further purification. HCl(g) was bubbled into methanol (4 mL) for 10 min. Then a solution of crude cyanohydrin (**4a/4b**) (450 mg, 1.04 mmol) in methanol−dioxane (2:1, 3 mL) was added to the HCl−methanol solution at 0 °C. The reaction mixture was sealed, stirred at 0 °C for 2 h, and then placed in a refrigerator for 48 h. The mixture was warmed to room temperature, and then 6 N HCl was added carefully. The mixture was stirred for 30 min and then concentrated to dryness. The resulting residue was dissolved in a 50% methanol−water solution, stirred overnight at room temperature, and then concentrated to dryness. The product was purified by flash chromatography on silica gel using hexanes−ethyl acetate (1:1) to yield *epi*-K252a **5** as an off-white solid. MS (ESI) *m/e* 468 (M + H); ^1H NMR ($CDCl_3$) δ 2.42 (s, 3H, 2.77 (dd, 1H), 2.91 (s, 3H), 2.95 (dd, 1H), 4.99 (s, 2H), 7.13 (dd, 1H), 7.33 (t, 1H), 7.44 (dd, 2H), 7.64 (t, 2H), 7.98 (d, 1H), 9.16 (d, 1H); HRFAB-MS calcd for $C_{27}H_{21}N_3O_5$, 468.1559; found 468.1558. Anal. $C_{27}H_{21}N_3O_5 \cdot 0.66H_2O$, C, H, N.

Amide **(3′*S*)-6** was obtained by eluting the column with ethyl acetate to give a light orange solid. MS (ESI) *m/e* 453 (M + H); ^1H NMR (DMSO-d_6) δ 2.33 (s, 3H), 2.87 (m, 1H), 4.94 (s, 2H), 6.58 (s, 1H), 7.19−7.64 (m, 6H), 7.81 (m, 3H), 7.96 (d, 1H), 8.59 (s, 1H), 9.17 (d, 1H); HRFAB-MS calcd for $C_{26}H_{20}N_4O_4$, 453.1563; found 453.1583.

Compound 8. Compound **7**[18] was dissolved in trimethyl phosphite (2 mL) and heated to reflux for 3 h. The reaction mixture was cooled to room temperature and flushed through a flash silica gel column using chloroform−methanol (20:1) to remove trimethyl phosphite. The product was purified by flash chromatography (silica gel; ethyl acetate:hexane; 1:1) to give compound **8** as a pale yellow solid (95% yield). MS (ESI^+): *m/e* 406 $(M + H)^+$, ^1H NMR ($CDCl_3$) δ 2.62 (s, 3H), 2.85 (d, 1H), 3.37−3.45 (m, 1H), 4.95 (s, 1H), 5.00 (s, 2H), 5.09 (s, 1H), 6.29 (s, 1H), 6.90 (d, 1H), 7.33−7.53 (m, 5H), 7.91 (d, 1H), 9.41 (d, 1H).

Compound (3′*R*)-10. To a stirred solution of **8** (350 mg, 0.67 mmol) in THF (10 mL) at room temperature under nitrogen was sequentially added pyridine (0.44 mL, 5.39 mmol) and osmium tetroxide (6.73 mL, 0.67 mmol, 0.1 M soln. in CCl_4). The yellow mixture was stirred at room-temperature overnight. After 36 h, aqueous sodium bisulfite solution (concentrated 30 mL) was added and the contents were stirred for 30 min, then extracted with EtOAc (2 × 20 mL), dried over sodium sulfate, filtered and concentrated in vacuo to a light brown film. The product was purified by flash chromatography on silica gel using ethyl acetate to yield a yellow solid (280 mg, 76%). MS (ESI) *m/e* 544 (M + H), ^1H NMR ($CDCl_3$) δ 0.56 (d, 6H), 1.079 (s, 9H), 2.04 (dd, 1H), 2.12 (broad s, 1H), 2.40 (s, 3H), 2.86 (dd, 1H), 3.52 (broad s, 3H), 4.99 (s, 2H), 6.98 (dd, 1H), 7.32 (t, 1H), 7.39−7.46 (m, 4H), 7.97 (dd, 2H), 9.35 (d, 1H).

To a flask containing methanol (2 mL) at 0 °C under nitrogen was added acetyl chloride (4 drops). Compound **9** (40 mg, 0.072 mmol) in methanol (1 mL) was added dropwise to the solution of methanol−HCl. This mixture was stirred at 0 °C for 1 h and then warmed to room-temperature overnight. The solvent was removed in vacuo leaving **10** as a tan solid (21 mg, 66%). MS (ESI) *m/e* 440 (M + H); ^1H NMR ($CDCl_3$) δ 2.05 (dd, 1H), 2.43 (s, 3H), 2.90 (dd, 1H), 3.57 (s, 1H), 3.61 (s, 2H), 5.04 (s, 2H), 6.28 (s, 1H), 7.02 (dd, 1H), 7.33−7.54 (m, 6H), 7.95 (d, 1 H), 8.02 (d, 1H), 9.32 (d, 1H); HRFAB-MS calcd for $C_{26}H_{21}N_3O_4$, 440.1610; found 440.1622.

Compound 11. To a stirred solution of **9** (0.23 g, 0.42 mmol) in THF (10 mL) at 0 °C under nitrogen were added triethylamine (57.9 μl, 0.42 mmol), DMAP (25.4 mg, 0.208 mmol), and *p*-toluenesulfonyl chloride (79.1 mg, 0.42 mmol). The reaction mixture was stirred at 0 °C for 1 h and then slowly warmed to room-temperature overnight. Thin-layer chromatography analysis (hexanes−ethyl acetate, 2:1) showed the presence of starting material so the reaction mixture was warmed for an additional 1 h. The reaction was then diluted with ethyl acetate (30 mL) and washed with water (3 × 15 mL). The organic phase was dried over sodium sulfate, filtered, and concentrated in vacuo to a yellow film. The product was purified by flash chromatography on silica gel using hexanes−ethyl acetate (2:1) to give **11** as a light yellow film (0.16 g, 55%) and starting material (0.8 g, 35% yield). MS (APCI) *m/e* 708 (M + H); ^1H NMR ($CDCl_3$) δ 0.57 (d, 6 H), 1.08 (s, 9H), 2.01 (dd, 1H), 2.33 (s, 3H), 2.42 (s, 3H), 3.88 (dd, 1H), 3.86 (dd, 2H), 4.98 (s, 2H), 6.97 (dd, 1H), 7.14 (d, 2H), 7.24−7.49 (m, 7H), 7.75 (d, 1H), 7.91 (d, 1H), 9.35 (d, 1H).

Compound (3′*R*)-12. To a stirred solution of **11** (0.14 g, 0.20 mmol) in THF (5 mL) at 0 °C under nitrogen was added sodium hydride (15.8 mg, 0.40 mmol). After vigorous evolution of hydrogen the reaction mixture became cloudy. Thin-layer chromatography analysis showed product and starting material. Additional sodium hydride (2 equiv) was then added, and the contents of the flask were stirred for an additional 2 h and then warmed gently for 4 h. The reaction mixture was then cooled to 0 °C, quenched with water, diluted with ethyl acetate, and washed with water and brine. The organic phase was dried over sodium sulfate, filtered, and concentrated in vacuo to a yellow film (100 mg, 95%). MS (APCI) *m/e* 536 (M + H); ^1H NMR ($CDCl_3$) δ 0.56 (d, 6H), 1.08 s, 9H), 2.32−2.38 (m, 4H), 2.57 (d, 2 H), 3.01 (dd, 1H), 4.99 (s, 2H), 7.01 (d, 1H), 7.33−7.56 (m, 5H), 7.73 (d, 1H), 7.94 (d, 1H), 9.46 (d, 1H).

Compound (3′*S*)-14. To a stirred solution of **12** (100 mg, 0.19 mmol) in THF (5 mL) at 0 °C under nitrogen was added

2 equiv of lithium triethylborohydride (0.37 mL of a 1 M solution in THF, 0.37 mmol) dropwise with evolution of gas. An additional 2 equiv of lithium triethylborohydride was added, and the reaction was stirred at 0 °C for 30 min and then warmed to room temperature. The reaction mixture was cooled to 0 °C and quenched with water, diluted with ethyl acetate, and washed with water and brine. The organic phase was dried over magnesium sulfate, filtered, and concentrated in vacuo. The product was purified by flash chromatography on silica gel using hexanes−ethyl acetate (1:1) to give **13** as a pale yellow film (90.8 mg, 91%). A methanol−HCl solution, prepared by adding acetyl chloride (5 drops) to methanol (2 mL), was added to a stirred solution of **13** in methanol at 0 °C under nitrogen. The reaction mixture was stirred at 0 °C for 30 min and then allowed to warm to room-temperature overnight. The solvent was removed in vacuo leaving a yellow solid, which was purified by silica gel chromatography using hexanes−ethyl acetate (1:1) to give **14** (30 mg, 42%). MS (ESI) *m/e* 424 $(M + H)^+$, ^{1}H NMR ($CDCl_3$) δ 1.39 (s, 3H), 2.29 (dd, 1H), 2.37 (s, 3H), 2.91 (dd, 1H), 5.05 (s, 2H), 6.19 (s, 1H), 6.97 (t, 1H), 7.32−7.50 (m, 5H), 7.78 (d, 1H), 7.95 (d,1H), 9.33 (d, 1H); HRFAB-MS calcd for $C_{26}H_{21}N_3O_3$, 424.1661; found 424.1656. Anal. $C_{26}H_{23}N_3O_3$, C, H, N.

Compound (3′*R*)-17. To a stirred solution of **16** (90.1 mg, 0.15 mmol) in THF (4 mL) at 0 °C under nitrogen was added lithium triethylborohydride (0.45 mL of a 1 M soln in THF, 0.45 mmol) slowly dropwise. The reaction mixture was stirred at 0 °C for 1 h and then slowly warmed to room-temperature overnight. The mixture was cooled to 0 °C, quenched with methanol, stirred at 0 °C for 15 min, and then warmed to room temperature. The solvent was removed in vacuo, leaving a yellow oil. The product was purified by flash chromatography on silica gel using ethyl acetate−hexane (1:1) to give **17** as a white solid (75 mg, 83%). MS (ESI) *m/e* 424 (M + H); ^{1}H NMR ($CDCl_3$) δ 1.69 (s, 3H), 1.99 (s, 3H), 2.86 (dd, 1H), 3.03 (dd, 1H), 4.37 (m, 3H), 4.93 (s, 2H), 6.43 (t, 1H), 6.95 (d, 1H), 7.03 (t, 1H), 7.18 (t, 1H), 7.44 (t, 1H), 7.79 (d, 1H), 7.99 (d, 1H), 8.69 (d, 1H); HRFAB-MS calcd for $C_{26}H_{21}N_3O_3$, 424.1661; found 424.1663.

Protein Kinase C Multiscreen "In-Plate" Assay. Protein kinase C activity was assessed using the Millipore Multiscreen TCA "in-plate" assay as previously described.[24,15a,b,16] Assays were performed in 96-well Multiscreen-DP plates (Millipore Cat. # MADPNOB50). Each 40-μL assay mixture contained 20 mM HEPES, pH 7.4, 10 mM $MgCl_2$, 2.5 mM EGTA, 2.5 mM $CaCl_2$, 80 μg/mL phosphatidylserine, 3.2 μg/mL diolein, 200 μg/mL histone H-1 (Fluka Cat. # 53412), 5 μM [γ-^{32}P]ATP (K_m level), 1.5 ng of PKC (UBI Cat. # 14508; mixed isozymes of α, β, γ), 0.1% BSA, 2% DMSO, and various concentrations of test compound. The reaction was allowed to proceed for 10 min at 37 °C and then quenched by adding 25 μL of ice-cold 50% trichloroacetic acid. The plates were allowed to equilibrate for 30 min at 4 °C and then washed 4× with 200 μL of ice cold 25% TCA. After being washed, the plates were removed from the vacuum manifold and the bottom of each plate was blotted. The flexible plate underdrain was removed, and the bottom was again blotted to remove any excess liquid. The plates were then placed in Wallac cassette holders with the bottom sealed with adhesive tape (Wallac Cat. # 1450-462). SuperMix (Cat. # 1200-439) scintillation cocktail (25 μL/well) was added, and the top of the plate was sealed with adhesive tape. The samples were equilibrated for 1 h prior to counting. The radioactivity was determined in the Wallac MicroBeta 1450 PLUS scintillation counter by using a protocol that has been previously normalized for counting ^{32}P in Millipore opaque plates.

Inhibition of trkA Tyrosine Kinase Activity. Compounds were evaluated for their ability to inhibit the kinase activity of baculovirus-expressed human trkA cytoplasmic domain using an ELISA-based assay as previously described.[9] The 96-well microtiter plate is coated with substrate solution (recombinant human phospholipase C-γl/glutathione S-transferase fusion protein.[25] Inhibition experiments were performed in 100 μL assay mixtures containing 50 mM HEPES, pH 7.4, 40 μM ATP, 10 mM $MnCl_2$ 0.1% BSA, 2% DMSO, and various concentrations of inhibitor. The reaction is initiated by addition of trkA kinase and allowed to proceed for 15 min at 37 °C. An antibody to phosphotyrosine (UBI) is then added, followed by a secondary enzyme-conjugated antibody, alkaline phosphatase-labeled goat antimouse IgG (Bio-Rad). The activity of the bound enzyme is measured via an amplified detection system (Gibco-BRL). Inhibition data are analyzed using the sigmoidal dose−response (variable slope) equation in GraphPad Prism.

VEGF-R2 Receptor-Linked Tyrosine Kinase Assay. Enzyme inhibition studies were performed as described previously[26] using a modification of the ELISA described for trkA kinase.[9] The 96-well microtiter plate (FluoroNUNC or Costar High Binding) was coated with 10 μg/mL recombinant human PLC-γ/GST. Kinase assays were performed in 100 μL reaction mixtures containing 50 mM HEPES (pH 7.4), K_m level of ATP, 10 mM $MnCl_2$, 0.1% BSA, 2% DMSO, and various concentrations of drug. The reaction was initiated by adding baculoviral recombinant human enzyme VEGF-R2 and allowed to proceed for 15 min at 37 °C. The detection antibody, Eu-N1 anti-phosphotyrosine (PT66) antibody, was added, and the plate was gently agitated. After 5 min, the fluorescence of the resulting solution was measured using the Victor Multilabel Counter.

trkA Cell-Based Autophosphorylation Assay. The inhibition of NGF-stimulated phosphorylation of trk was performed, essentially as described previously.[21a] NIH3T3 cells transfected with trkA (NIH3T3-trkA) were plated in 100-mm tissue culture dishes. Subconfluent cells were then serum-starved by replacing media with serum-free DMEM-containing 0.05% BSA. At this point, test compounds were added to the NIH3T3-trkA cells and incubated for 1 h at 37 °C. Except for the negative control, NGF (10 ng/mL) was added to the positive control and compound-treated cells. After 5 min of ligand stimulation, the cells were rinsed with ice-cold PBS and then lysed with RIPA buffer containing 10 mM Tris(HCl), pH 7.2, 150 mM NaCl, 1% Triton X-100, 1% sodium deoxycholate, 0.1% sodium dodecyl sulfate (SDS), protease inhibitors, and 1 mM sodium vanadate. Immunoprecipitation and immunoblotting were then performed as previously described.[21b] Clarified cell lysates corresponding to equal amounts of protein were immunoprecipitated with anti-trk antibody for 1 h, followed by incubation with Protein A-Sepharose for another hour at 4 °C. Immunoprecipitates were washed with lysis buffer, analyzed on a 7.5% SDS-polyacrylamide gel, and then transferred onto Millipore PVDF membrane. The membrane was immunoblotted with 4G10 anti-phosphotyrosine antibody, followed by incubation with horseradish peroxidase coupled goat anti-mouse IgG. Phosphorylated bands were visualized by enhanced chemiluminescence.

Supporting Information Available: HPLC and C, H, N analysis. This material is available free of charge via the Internet at http://pubs.acs.org.

References

(1) (a) Glass, D. J.; Yancopoulos, G. D. The neurotrophins and their receptors. *Trends Cell Biol*. **1993**, *3*, 262−268. (b) Meakin, S. O.; Shooter, E. M. The nerve growth factor family of receptors. *Trends Neurosci*. **1992**, *15*, 323−331. (c) Lee, F. S.; Kim, A. H.; Khursigara, G.; Chao, M. V. The uniqueness of being a neurotrophin receptor. *Curr. Opin. Neurobiol*. **1994**, *25*, 1349−1361. (d) Ross, A. H. Identification of tyrosine kinase Trk as a nerve growth factor receptor. *Cell Regul*. **1991**, *2*, 685−690. (e) Ullrich, A.; Schlessinger, J. Signal transduction by receptor with tyrosine kinase activity. *Cell* **1990**, *61*, 203−212. (f) Kaplan, D. R.; Hempstead, B. L.; Martin-Zanca, D.; Chao, M. V.; Parada, L. F. The trk proto-oncogene product: a signal transducing receptor for nerve growth factor. *Science* **1991**, *252*, 554−558.

(2) Kaplan, D. R.; Stephens, M. R. Neurotrophin signal transduction by the Trk receptor. *J. Neurobiol*. **1994**, *25*, 1404−1417.

(3) (a) Thoenen, H.; Barde, Y. A. Physiology of nerve growth factor. *Physiol. Rev*. **1980**, *60*, 1284−1335. (b) DiStefano, P. S. Pharmacology of neurotrophic factors in models of neurodegenerative diseases. *Annu. Rep. Med. Chem*. **1993**, *28*, 11−17. (c) Lad, S. P.; Neet, K. E.; Mufson, E. J. Nerve growth factor: structure, function and therapeutic implications for Alzheimer's disease. *Current Drug Targets- CNS and Neurological Disorders* **2003**, *2*, 315−334.

(4) (a) Ruggeri, B. A.; Miknyoczki, S. J.; Singh, J.; Hudkins, R. L. Role of Neurotrophin-Trk interactions in oncology: the antitumor efficacy of potent and selective trk tyrosine kinase inhibitors in pre-clinical tumor models. *Curr. Med. Chem.* **1999**, *6*, 845−857. (b) Miknyoczki, S. J.; Klein-Szanto, A. J. P.; Ruggeri, B. A. Neurotrophin-trk receptor interactions in neoplasia: a possible role in interstitial and perineural invasion in ductal pancreatic cancer. *Crit. Rev. Oncog.* **1996**, *7*, 89−100. (c) Miknyoczki, S. J.; Lang, L.; Klein-Szanto, A. J. P.; Dionne, C. A.; Ruggeri, B. A. Neurotrophins and trk receptors in human pancreatic ductal adrenocarcinoma: Expression patterns and effects on in vitro invasive behavior. *Int. J. Cancer* **1999**, *81*, 417−427. (d) Miknyoczki, S. J.; Wan, W.; Chang, H.; Dobrzanski, P.; Ruggeri, B. A.; Dionne, C. A.; Buchkovich, K. The neurotrophin-trk receptor axes are critical for the growth and progression of human prostatic carcinoma and pancreatic ductal adenocarcinoma xenographs in nude mice. *Clin. Cancer Res*. **2002**, *8*, 1924−1931. (e) Pflug, B. R.; Dionne, C.; Kaplan, D. R.; Lynch, J.; Djakiew, D. Expression of a high affinity nerve growth factor receptor in the human prostate. *Endocrinology* **1995**, *136*, 262−268.

(5) Tagliabue, E.; Castiglioni, F.; Ghirelli, C.; Modugno, M.; Asnaghi, L.; Somenzi, G.; Melini, C.; Menard, S. Nerve growth factor cooperates with p185(HER2) in activating growth of human breast carcinoma cells. *J. Biol. Chem*. **2000**, *275*, 5388−5394.

(6) (a) Djakiew, D.; Delsite, R.; Pflug, B.; Wrathall, J.; Lynch, J. H.; Onoda, M. Regulation of growth by a nerve growth factor-like protein which modulates paracrine interactions between a neoplastic epithelial cell line and stromal cells of the human prostate. *Cancer Res*. **1991**, *51*, 3304. (b) Weeraratna, A. T.; Dalrymple, S. L.; Lamb, J. C.; Denmeade, S. R.; Miknyoczki, S.; Dionne, C. A.; Isaacs, J. T. Pan-trk inhibition decreases metastasis and enhances host survival in experimental models due to its selective induction of apoptosis of prostate cancer cell. *Clin. Cancer Res*. **2001**, *7*, 2237−2245. (c) Weeraratna, A. T.; Arnold, J. T.; George, D. J.; DeMarzo, A.; Isaacs, J. T. Rational basis for trk inhibition therapy for prostate cancer. *Prostate* **2000**, *45*, 140−148. (d) Weeraratna, A. T.; Dalrymple, S. L.; Lamb, J. C.; Denmeade, S. R.; Miknyoczki, S.; Dionne, C. A.; Isaacs, J. T. Pan-trk inhibition decreases metastasis and enhances host survival in experimental models due to its selective induction of apoptosis of prostate cancer cell. *Clin. Cancer Res*. **2001**, *7*, 2237−2245.

(7) (a) Sezaki, M.; Sasaki, T.; Nakazawa, T.; Takeda, U.; Iwata, M.; Watanabe, T.; Koyama, M.; Kai, F.; Shomura, T.; Kojima, M. A new antibiotic SF-2370 produced by Actinomadura. *J. Antibiot*. **1985**, *38*, 1437−1439. (b) Kase, H.; Iwahashi, K.; Matsuda, Y. K-252a, a potent inhibitor of protein kinase C from microbial origin. *J. Antibiot*. **1986**, *39*, 1059−1065. (c) Yasuzawa, T.; Iida, T.; Yoshida, M.; Hirayama, N.; Takahashi, M.; Shirahata, K.; Sano, H. The structures of novel protein kinase c inhibitors K252a, b, c, and d. *J. Antibiot*. **1986**, *39*, 1072−1078.

(8) Angeles, T. S.; Yang, S. X.; Steffler, C.; Dionne, C. A.; Kinetics of trkA tyrosine kinase activity and inhibition by K-252a. *Arch. Biochem. Biophys*. **1998**, *349*, 267−274.

(9) Angeles, T. S.; Steffler, C.; Bartlett, B. A.; Hudkins, R. L.; Stephens, R. M.; Kaplan, D. R.; Dionne, C. A. Enzyme-linked immunosorbent assay for trkA tyrosine kinase activity. *Anal. Biochem*. **1996**, *206*, 49−55.

(10) (a) Berg, M. M.; Sternberg, D. W.; Parada, L. F.; Chao, M. V. K-252a inhibits nerve growth factor-induced *trk* proto-oncogene tyrosine phosphorylation and kinase activity. *J. Biol. Chem.* **1992**, *267*, 13−16. (b) Tarpley, P. Lamballe, F., Barbacid, M. K-252a is a selective inhibitor of the tyrosine protein kinase activity of the *trk* family of oncogenes and neurotrophin receptors. *Oncogene* **1992**, *7*, 371−381. (c) Ohmichi, M.; Decker, S. J.; Pang, I.; Saltiel, A. R. Inhibition of the cellular actions of nerve growth factor by staurosporine and K-252a results from the attenuation of the activity of the *trk* tyrosine kinase. *Biochemistry* **1992**, *31*, 4034−4039. (d) Muroya, K.; Hashimoto, Y.; Hattori, S.; Nakamuru, S. Specific inhibition of NGF receptor tyrosine kinase activity by K-252a. *Biochim. Biophys. Acta* **1992**, *1135*, 353−356. (e) Nye, S. H.; Squinto, S. P.; Glass, D. J.; Stitt, T. N.; Hantzopoulos, P.; Macchi, M. J.; Lindsaay, N. S.; Ip, N. Y.; Yancopoulos, G. D. K-252a and staurosporine selectively block autophosphorylation of neurotrophin receptors and neurotrophin-mediated responses. *Mol. Biol. Cell* **1992**, *3*, 677−683.

(11) Knusel, B.; Hefti, H. K-252 compounds: modulators of neurotrophin signal transduction. *J. Neurochem*. **1992**, *59*, 1987−1995.

(12) (a) Hudkins, R. L.; Iqbal, M.; Park, C.-H.; Goldstein, J.; Herman, J. L.; Shek, E.; Murakata, C.; Mallamo, J. P. Prodrug esters of the indolocarbazole CEP-751. *Bioorg. Med. Chem. Lett*. **1998**, *8*, 1873−1876. (b) Dionne, C.; Camoratto, A.; Jani, J.; Emerson, E.; Neff, N.; Vaught, J.; Murakata, C.; Djakiew, D.; Lamb, J.; Bova, S.; George, D.; Isaacs, J. Cell cycle independent-death of prostate adenocarcinoma is induced by trk tyrosine kinase inhibitor CEP-751 (KT6587). *Clin. Cancer Res*. **1998**, *4*, 1887−1898. (c) Camoratto, A. M.; Jani, J. P.; Angeles, T. S.; Maroney, A. C.; Sanders, C. Y.; Murakata, C.; Neff, N. T.; Vaught, J. L.; Isaacs, J. T.; Dionne, C. A. CEP-751 inhibits trk receptor tyrosine kinase activity *in vitro* and exhibits anti-tumor activity. *Int. J. Cancer* **1997**, *72*, 673−679.

(13) Miknyoczki, S. J.; Chang, H.; Klein-Szanto, A.; Dionne, C. A.; Ruggeri, B. A. The Trk tyrosine kinase inhibitor CEP-701 (KT-5555) exhibits significant antitumor efficacy in preclinical xenograft models of human pancreatic ductal adenocarcinoma. *Clin. Cancer Res.* **1945**, *5*, 2205−2212.

(14) George, D. J.; Dionne, C. A.; Jani, J.; Angeles, T.; Murakata, D.; Lamb, J.; Isaacs, J. T. Sustained *in vivo* regression of Dunning H rat prostate cancers treated with combinations of androgen ablation and trk tyrosine kinase inhibitors, CEP-751 (KT-6587) or CEP-701 (KT-5555). *Cancer Res.* **1999**, *59*, 2395−2401.

(15) (a) Kaneko, M.; Saito, Y.; Saito, H.; Matsumoto, T.; Matsuda, Y.; Vaught, J. L.; Dionne, C. A.; Angeles, T. S.; Glicksman, M. A.; Neff, N. T.; Rotella, D. P.; Kauer, J. C.; Mallamo, J. P.; Hudkins, R. L.; Murakata, C. Neurotrophic 3,9-bis[(alkylthiomethyl]- and -[bis(alkoxymethyl)]-K-252a derivatives. *J. Med. Chem.* **1997**, *40*, 1863−1869. (b) Murakata, C.; Kaneko, M.; Gessner, G.; Angeles, T. S.; Ator, M. A.; O'Kane, T. M.; McKenna, B. A. W.; Thomas, B. A.; Mathiasen, J. R.; Saporito, M. S.; Bozyczko-Coyne, D.; Hudkins, R. L. Mixed lineage kinase activity of indolocarbazole analogs. *Bioorg. Med. Chem. Lett.* **2002**, *12*, 147−150. (c) Dionne, C. A.; Contreras, P. C.; Murakata, C. Use of indolocarbazole derivatives to treat a pathological condition of the prostate. US 5516771.

(16) Gingrich, D. E.; Hudkins, R. L. Synthesis and kinase inhibitory activity of 3′-(*S*)-*epi*-K-252a. *Bioorg. Med. Chem. Lett*. **2002**, *12*, 2829−2831.

(17) (a) Hudkins, R. L.; Gingrich, D. 3′-Epimeric K-252 derivatives. US 6093713. (b) Hudkins, R. L.; Gingrich, D. 3′-Epimeric K-252 derivatives for treating neurological disorders and cancer. US 6451786.

(18) Murakata, C.; Sato, A.; Takahashi, M.; Kobayashi, E.; Morimoto, M.; Akinaga, S.; Hirata, T.; Mochida, K.; Kase, H.; Yamada, K.; Iwashashi, K. US 4923986.

(19) Corey, E. J.; Winter, R. A. E. A new stereospecific olefin synthesis from 1,3-diols. *J. Am. Chem. Soc*. **1963**, *85*, 2677−2680.

(20) Goekjian, P. G.; Jirousek, M. R. Protein kinase C in the treatment of disease: signal transduction pathways, inhibitors, and agents in development. *Curr. Med. Chem*. **1999**, *6*, 877−903.

(21) (a) Maroney, A. C.; Sanders, C.; Neff, N. T.; Dionne, C. A. K-252b potentiation of neurotrophin-3 is trkA specific in cells lacking $p75^{NTR}$. *J. Neurochem*. **1997**, *68*, 88−94. (b) Maroney, A. C.; Lipfert, L.; Forbes, M. E.; Glicksman, M. A.; Neff, N. T.; Siman, R.; Dionne, C. A. K-252a induces tyrosine phosphorylation of the focal adhesion kinase and neurite outgrowth in human neuroblastoma SH−SY5Y cells. *J. Neurochem*. **1995**, *64*, 540−549.

(22) Schierling, N.; Knapp, S.; Marconi, M.; Flocco, M. M.; Cui, J.; Pergeo, R.; Rusconi, L.; Cristiani, C. Crystal structure of the tyrosine kinase domain of the hepatocyte growth factor receptor c-met and its complex with the microbial alkaloid K-252a. *PNAS*, **2003**, *100*, 12654−12659.

(23) Mohammadi, M.; McMahon, G.; Sun, L. Tang, C.; Hirth, P.; Yeh, B. K.; Hubbard, S. R.; Schlessinger, J. Structure of the tyrosine kinase domain of fibroblast growth factor receptor in complex with inhibitors. *Science* **1997**, *276*, 955−960.

(24) Pitt, A. M.; Lee, C. High throughput screening protein kinase assays optimized for reaction, binding, and detection totally within a 96-well plate. *J. Biomol. Screening* **1996**, *1*, 47−51.

(25) Rotin, D.; Margolis, B.; Mohammadi, M.; Daly, R. J.; Daum, G.; Li, N.; Fischer, E. H.; Burgess, W. H.; Ullrich, A.; Schlessinger, J. SH2 domains prevent tyrosine dephosphorylation of the EGF receptor: identification of Tyr992 as the high-affinity binding site for SH2 domains of phospholipase C gamma. *EMBO J*. **1992**, *11*, 559−567.

(26) Gingrich, D. E.; Reddy, D. R.; Iqbal, M. A.; Singh, J.; Aimone, L. D.; Angeles, T. S.; Albom, M.; Yang, S.; Meyer, S.; Robinson, C.; Ruggeri, B. A.;. Dionne, C. A.; Vaught, J. L.; Mallamo, J. P.; Hudkins, R. L. A new class of potent VEGF receptor tyrosine kinase inhibitors: structure−activity relationships for a series of 9-alkoxymethyl-12-(3-hydroxypropyl)-indeno[2,1-a]pyrrolo[3,4-c]carbazole-5-ones and the identification of CEP-5214 and its dimethylglycine ester prodrug clinical candidate CEP-7055. *J. Med. Chem*. **2003**, *46*, 5375−5388.

JM040178M